Aluminum Molecular Rings bearing Amino-polyalcohol for Iodine Capture

Yi Zhang,[#] Qiao-Hong Li,[#] Wei-Hui Fang* and Jian Zhang

State Key Laboratory of Structural Chemistry, Fujian Institute of Research on the Structure of Matter, Chinese Academy of Sciences, Fuzhou, Fujian 350002, P. R. China.
Email: fwh@fjirsm.ac.cn

CONTENT

Experimental Section

All the reagents and solvents employed were purchased commercially and used as received without further treatment. Aluminium isopropoxide, diisopropanolamine, 1,4-Butanediol were acquired from Aladdin Chemical Reagent Shanghai. Diethanolamine, phenol, methanol, and N, N-dimethylformamide (DMF) were acquired from Sinopharm Chemical Reagent Beijing. The Fourier transform infrared spectroscopy (FT-IR) data (KBr pellets) was recorded on a PerkinElmer Spectrum 100 FT-IR spectrometer over a range 400-4000 cm^{-1}. The energy dispersive spectroscopy (EDS) analyses of single crystals were performed on a JEOL JSM6700F field-emission scanning electron microscope equipped with an Oxford INCA system. The EDS mapping of single crystals after iodine adsorption were performed on a Zeiss Sigma 300 field-emission scanning electron microscope equipped with an OXFORD AZtecOne X-Max^N 20 silicon drift detector. Powder X-ray diffraction (PXRD) data were collected on a Rigaku Mini Flex II diffractometer using CuK radiation (λ = 1.54056 Å) under ambient conditions. The thermogravimetric analyses (TGA) were performed on a Mettler Toledo TGA/SDTA 851e analyzer in a nitrogen atmosphere with a heating rate of 10 ^{o}C/min. The confocal Raman spectra were recorded on Horiba Jobin Yvon Labram HR Evolution Raman spectrometer at 785nm.

Synthesis of AlOC-61.

A mixture of aluminium isopropoxide (500 mg, 2.45 mmol), diethanolamine (2 mL, 20.8 mmol), 1,4-Butanediol (2 mL) was sealed in a 20 mL vial and transferred to a preheated oven at 100 ^{o}C for 3 days. When cooled to room temperature, colourless crystals were obtained. (yield: 21 % based on Al(OiPr)$_3$). The crystals are rinsed with DMF and preserved under a sealed and dry environment. FT-IR (KBr, cm^{-1}): 3110(v), 2920(s), 2858(s), 2695(m), 1506(w), 1443(m), 1274(s), 1075(s), 825(m).

Synthesis of AlOC-62.

A mixture of aluminium isopropoxide (500 mg, 2.45 mmol), diisopropanolamine (1mL, 7.5 mmol), methanol (2 mL) and DMF (2 mL) was sealed in a 20 mL vial and transferred to a preheated oven at 80 ^{o}C for 3 days. When cooled to room temperature, colourless crystals were obtained. (yield: 38 % based on Al(O^{i}Pr)$_3$). The crystals are rinsed with ethanol and preserved in a sealed and dry environment. FT-IR (KBr, cm^{-1}): 3118(v), 2914(s), 2853(s), 1510(s), 1456(m), 1360(s), 1284(s), 1150(s), 831(m).

Synthesis of AlOC-63.

A mixture of aluminium isopropoxide (500 mg, 2.45 mmol), diethanolamine (2 mL, 20.8 mmol), phenol (2 mL), 1,4-Butanediol (2 mL) was sealed in a 20 mL vial and transferred to a preheated oven at 100 ^{o}C for 3 days. When cooled to room temperature, colourless crystals were obtained. (yield: 42 % based on Al(O^{i}Pr)$_3$). The crystals are rinsed with ethanol and preserved in a sealed and dry environment. The crystals are rinsed with IPA and preserved under a sealed and dry environment. FT-IR (KBr, cm^{-1}): 3480(v), 3110(v), 2920(s), 2852(s), 2695(v), 1655(v), 1506(w), 1450(m), 1365(s), 1271(s), 1131(s), 828(m).

Synthesis of AlOC-64.

A mixture of aluminium isopropoxide (500 mg, 2.45 mmol), diethanolamine (2 mL, 20.8 mmol), 1,4-Butanediol (2 mL) was sealed in a 20 mL vial and transferred to a preheated oven at 100 ^{o}C for 3 days. The obtained system was continued to react at room temperature for 8 days, it was observed that the colourless crystals changed from needle to block. Obtained **AlOC-64**. The crystals are rinsed with DMF and preserved under a sealed and dry environment. FT-IR (KBr, cm^{-1}): 3258(v), 2920(s), 2855(s), 2695(v),

1660(v), 1506(w), 1450(m), 1360(s), 1120(s), 825(m).

X-ray Crystallographic Analyses.

Crystallographic data of crystal **AlOC-61**, **AlOC-62**, **AlOC-63**, and **AlOC-64** were collected on Hybrid Pixel Array detector equipped with Ga-Kα radiation (λ = 1.3405 Å) at 100 K. The structures were solved with the dual-direct methods using ShelXT and refined with the full-matrix least-squares technique based on F^2 using the SHELXL-2014. Non-hydrogen atoms were refined anisotropically. Hydrogen atoms were added theoretically, riding on the concerned atoms and refined with fixed thermal factors. All absorption corrections were performed using the multiscan program. The diffused electron densities resulting from residual solvent molecules were removed from the data set using the *SQUEEZE* routine of *PLATON* and refined further using the data generated. The obtained crystallographic data are summarized in Table S1.

Table S1 Summary of aluminum molecular rings: crystal data and structure refinement results

Compound	AlOC-61	AlOC-62	AlOC-63	AlOC-64
Formula	$C_{48}H_{120}Al_{12}N_{12}O_{36}$	$C_{56}H_{104}Al_8N_8O_{24}$	$C_{48}H_{84}Al_6N_6O_{22}$	$C_{40}H_{100}Al_6N_6O_{26}$
Mr	1765.31	1489.31	1259.09	1243.13
Temperature(K)	100 K	100 K	100 K	100 K
Wavelength (Å)	1.34050	1.34050	1.34050	1.34050
Crystal system	trigonal	triclinic	trigonal	triclinic
Space group	P -3	P-1	P -3	P-1
a/Å	28.6072(7)	17.3306(2)	22.4999(6)	12.3873(4)
b/Å	28.6072(7)	17.6352(3)	22.4999(6)	12.7993(4)
c/Å	10.6348(3)	27.9553(4)	12.7820(3)	12.8165(4)
$α$/°	90	85.3990(10)	90	66.719(3)
$β$/°	90	75.2440(10)	90	72.747(3)
$γ$/°	120	80.3140(10)	120	70.308(3)
V/Å^3	7537.2(4)	8138.1(2)	5603.9(3)	1725.77(11)
Z	3	4	3	1
$ρ$/g cm^{-3}	1.167	1.216	1.119	1.196
$μ$/mm^{-1}	1.126	0.996	0.874	0.969
$F(000)$	2808.0	3168.0	2004.0	668.0
Collected reflns	33637	117233	21595	23055
Uniq reflns (R_{int})	11324(0.0302)	36587(0.0567)	6574(0.0363)	7779(0.0285)
Completeness	0.973	0.972	0.994	0.976
GOF on F^2	1.070	1.126	1.270	1.058
R_1[a]/wR_2[b][I >2(I)]	0.0862/0.2785	0.0752/0.2197	0.1139/0.3035	0.0647/0.1825
CCDC number	2117926	2117930	2117927	2117928

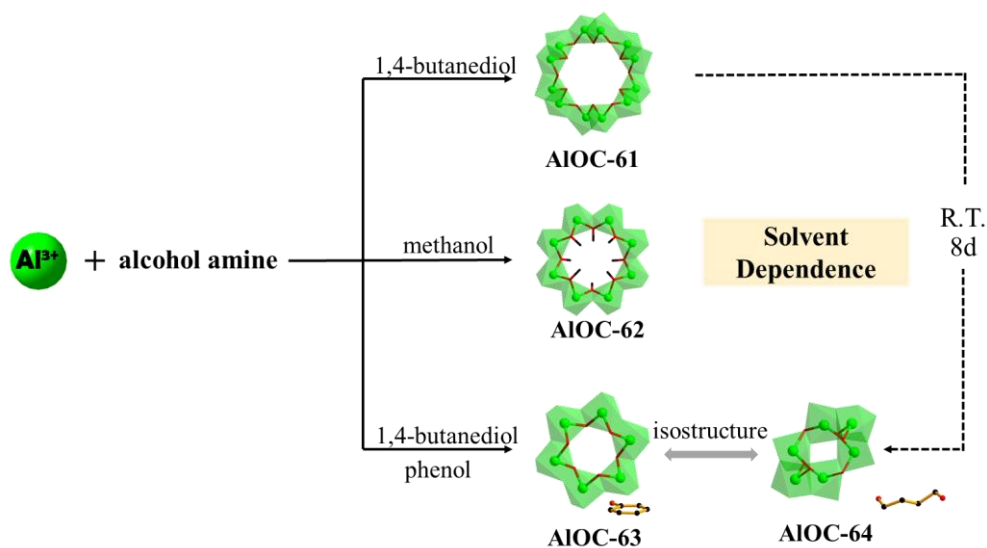[a]$R_1 = Σ||F_o|-|F_c||/Σ|F_o|$. [b]$wR_2 = \{Σ[w(F_o^2-F_c^2)^2]/Σ[w(F_o^2)^2]\}^{1/2}$.

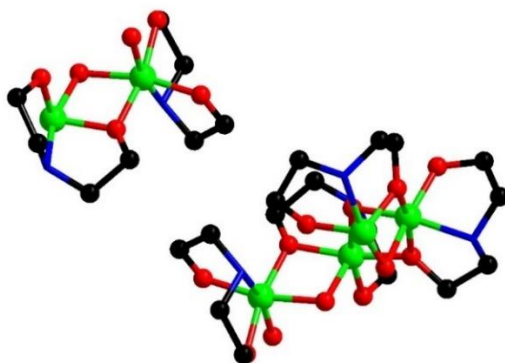**Fig. S1** Diagram showing the solvent dependence synthesis of the aluminium molecular rings.

Fig. S2 Two crystallographically independent moieties in the asymmetric unit of **AlOC-61**. Color code: Al, green; C, black; O, red; N, blue.
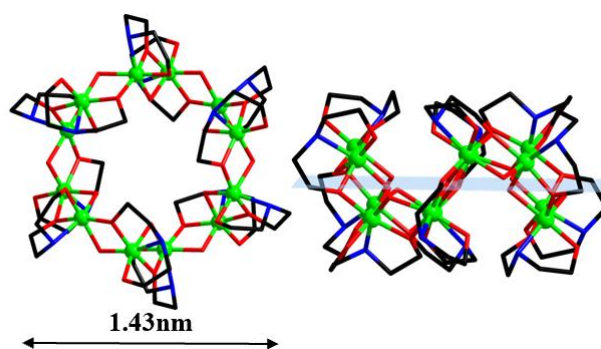

1.43nm

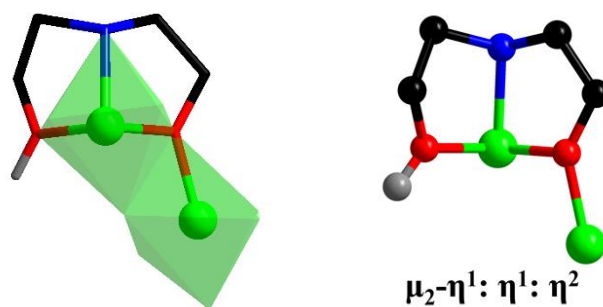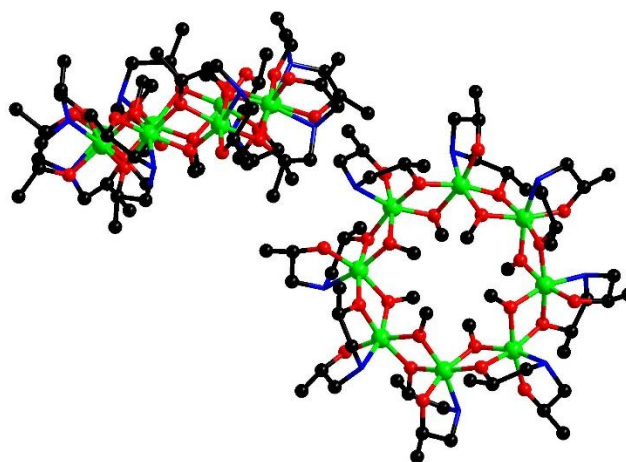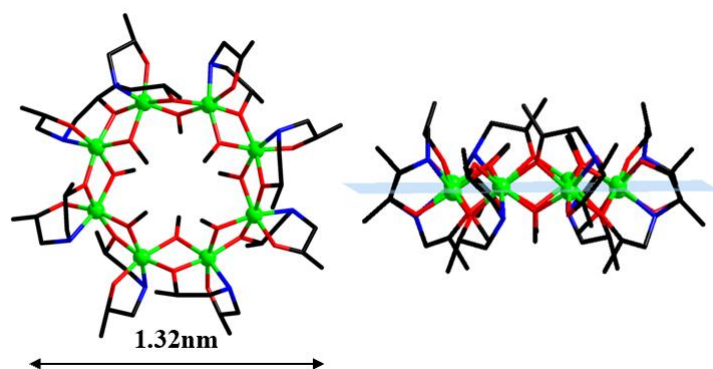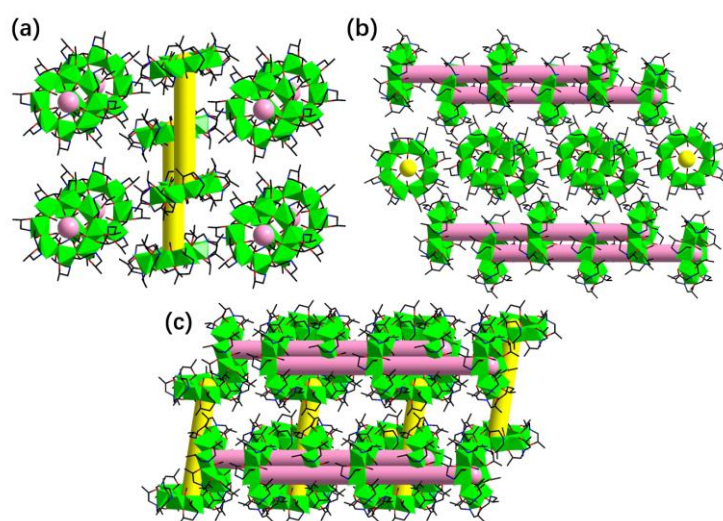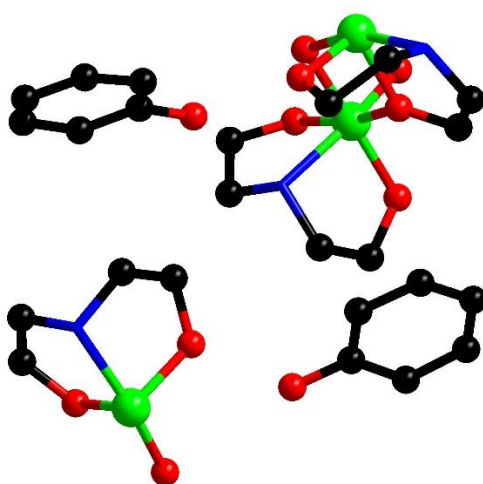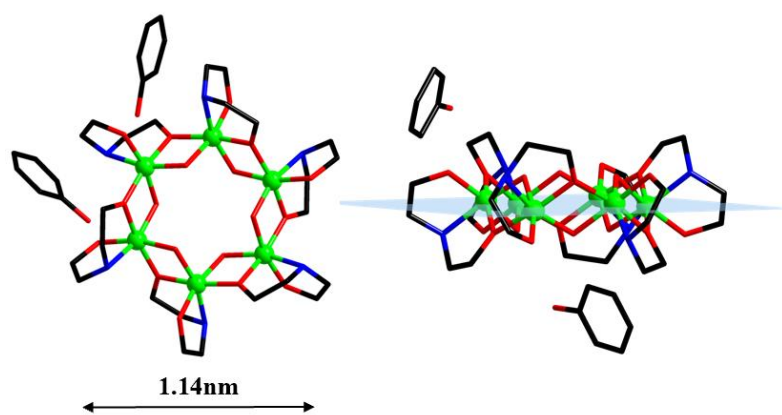**Fig. S3** Top (left) and side (right) view of **AlOC-61**. Color code: Al, green; C, black; O, red; N, blue.

Fig. S4 Coordination environment of Al^{III} ions in all Al rings: the μ_2-η^1: η^1: η^2 mode. Color code: Al, green; C, black; O, red; N, blue; H, gray.
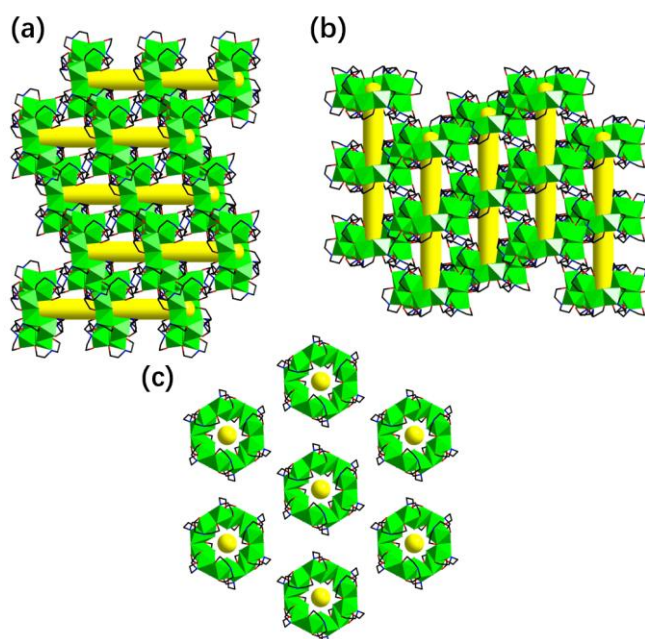
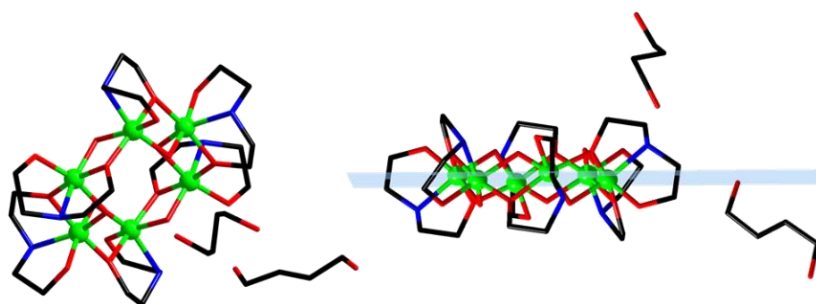**Fig. S5** Stacking diagrams of **AlOC-61** in the view of a-axis (a), b-axis (b) and c-axis (c).

Fig. S6 Two crystallographically independent moieties in the asymmetric unit of **AlOC-62**. Color code: Al, green; C, black; O, red; N, blue.

Fig. S7 Top (left) and side (right) view of **AlOC-62**. Color code: Al, green; C, black; O, red; N, b blue.

Fig. S8 Stacking diagrams of **AlOC-62** in the view of a-axis (a), b-axis (b) and c-axis (c).

Fig. S9 Crystallographically independent moieties in the asymmetric unit of **AlOC-63**. Color code: Al, green; C, black; O, red; N, blue.

Fig. S10 Top (left) and side (right) view of **AlOC-63**. Color code: Al, green; C, black; O, red; N, blue.
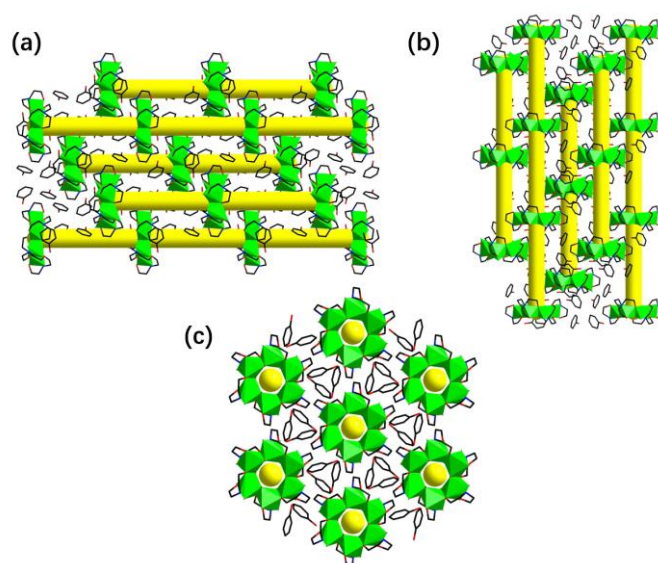
Fig. S11 Stacking diagrams of **AlOC-63** in the view of a-axis (a), b-axis (b) and c-axis (c).

Fig. S12 Top (left) and side (right) view of **AlOC-64**. Color code: Al, green; C, black; O, red; N, blue.
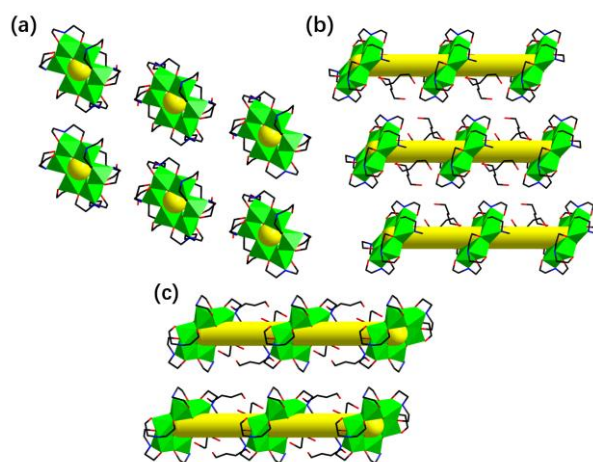
Fig. S13 Stacking diagrams of **AlOC-64** in the view of a-axis (a), b-axis (b) and c-axis (c).

PXRD analyses for molecular rings.
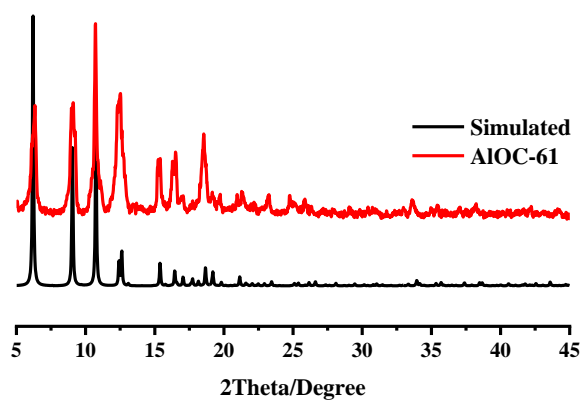
Fig. S14 PXRD patterns of **AlOC-61**.
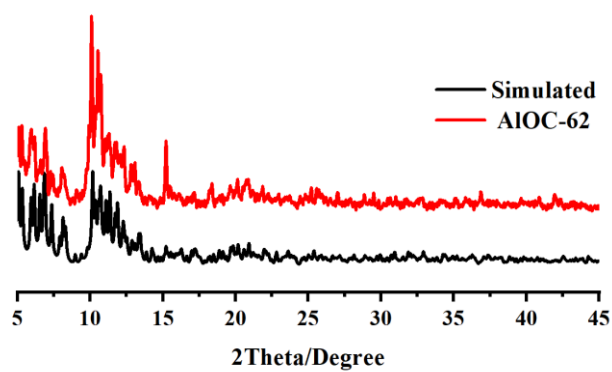
Fig. S15 PXRD patterns of **AlOC-62**.
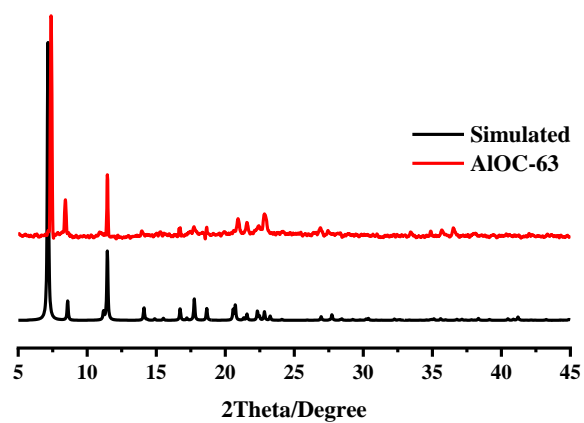
Fig. S16 PXRD patterns of **AlOC-63**.
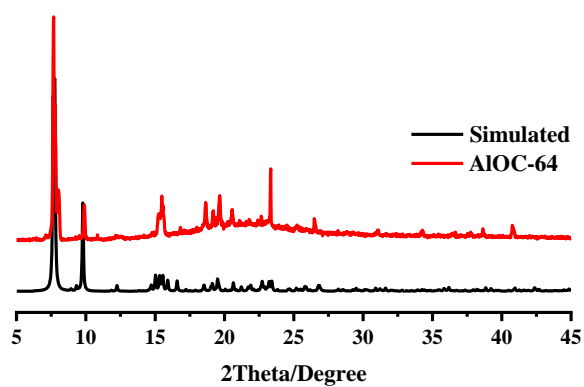
Fig. S17 PXRD patterns of **AlOC-64**.

FT-IR spectra of molecular rings.
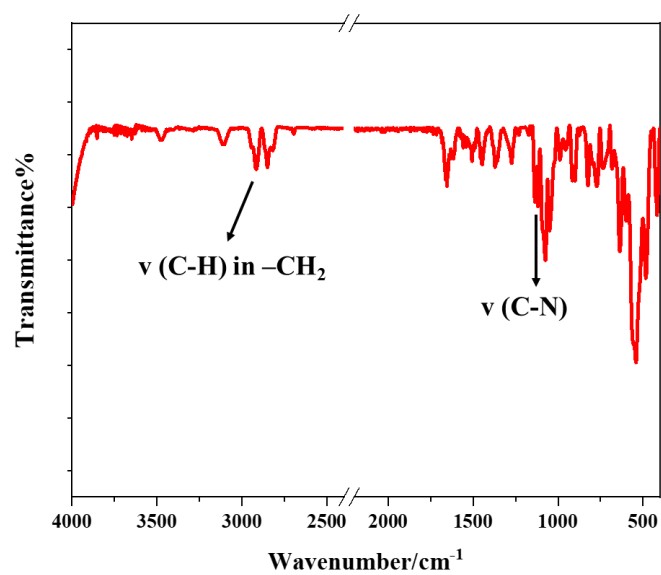
Fig. S18 FT-IR spectra of **AlOC-61**.
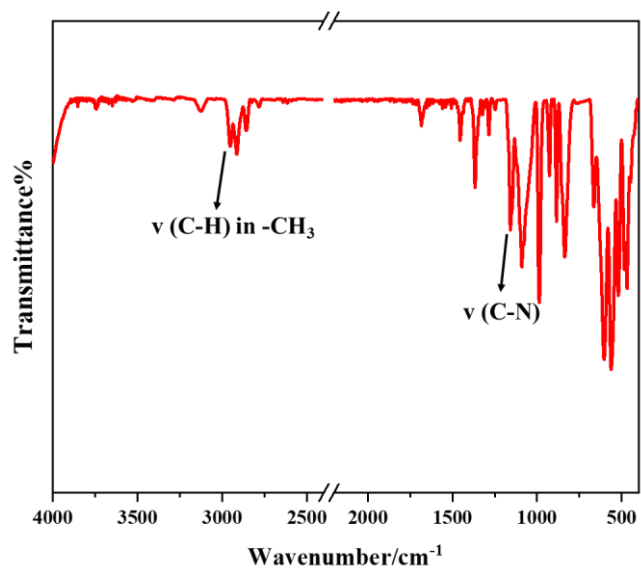
Fig. S19 FT-IR spectra of **AlOC-62**.
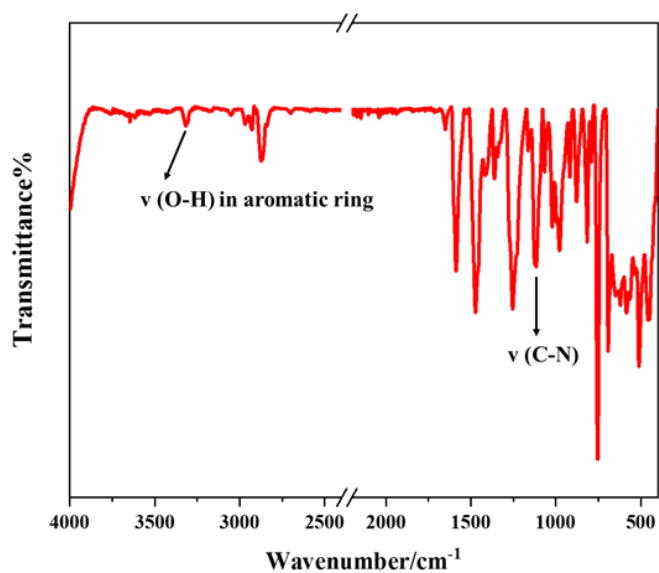
Fig. S20 FT-IR spectra of **AlOC-63**.
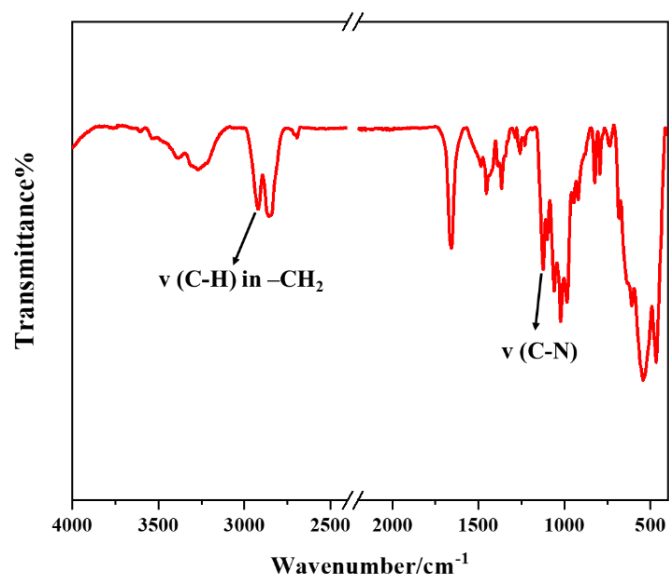
Fig. S21 FT-IR spectra of **AlOC-64**.

EDS spectra of molecular rings.
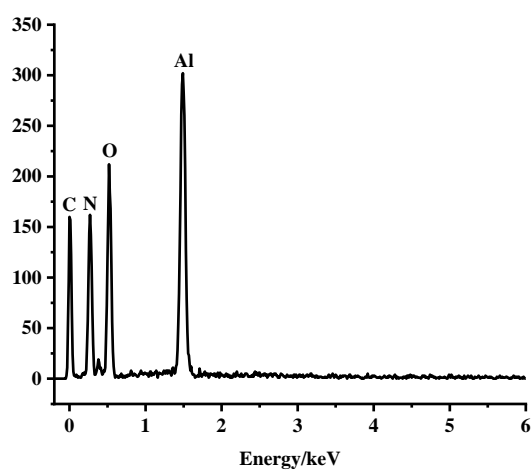
Fig. S22 EDS spectra of **AlOC-61**.
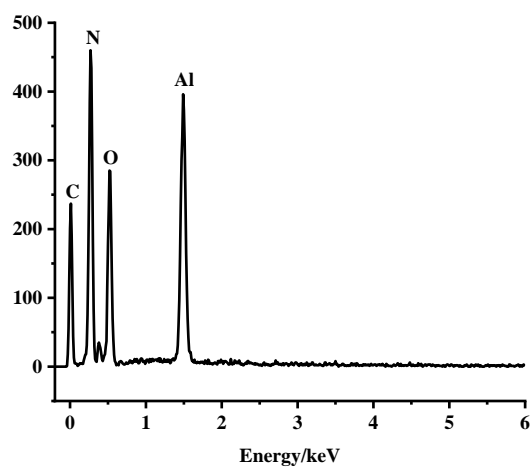
Fig. S23 EDS spectra of **AlOC-62**.
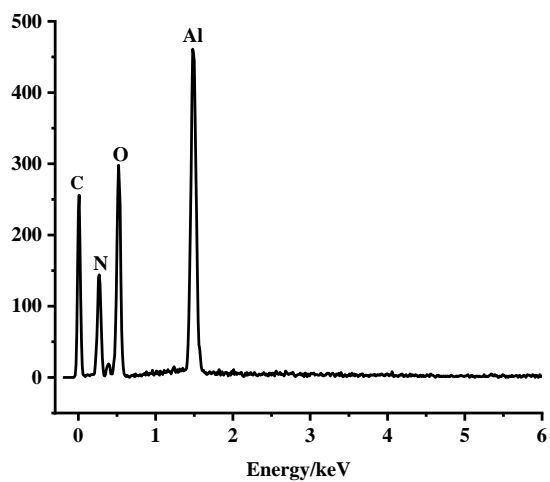
Fig. S24 EDS spectra of **AlOC-63**.
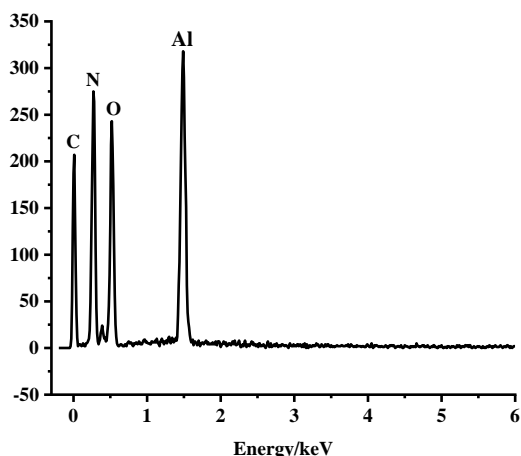
Fig. S25 EDS spectra of **AlOC-64**.

TGA spectra of molecular rings.
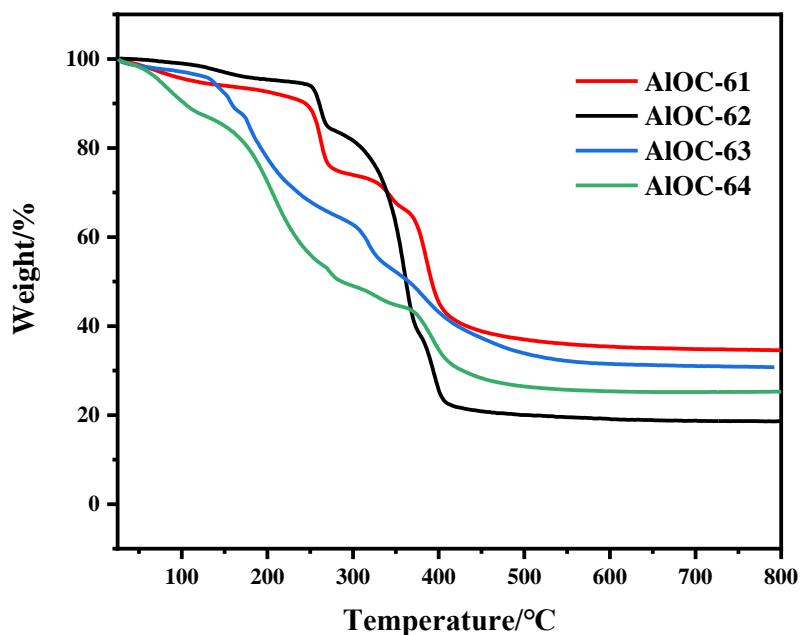
Fig. S26 TGA spectra of **AlOC-61**, **AlOC-62**, **AlOC-63** and **AlOC-64**.

Iodine/Cyclohexane Adsorption Measurement.

Adsorption studies were performed by immersing 10mg sample in 10 mL iodine/cyclohexane solution. The supernatant solution was used for each UV–vis absorbance measurement periodically. After each measurement, the solution was dispensed back into the respective vial to keep the volume constant. The absorbance at the maximum wavelength of iodine (λ_{max} = 521nm) was selected to calculate the iodine content, and the absorbance value of the original solution was standardized to 100%. The removal ratios of iodine were calculated using $R = (C_0 - C_t)/C_0 \times 100\%$ (where C_0 and C_t represent the initial concentration and concentration at time t, respectively).

Sorption kinetics of iodine in **AlOC-61** and **AlOC-63** were fitted to a pseudo-second-order kinetics model, respectively, $t/q_t = 1/h + t/q_e$ (where q_t, q_e represent the amounts of adsorbate at certain time t or at equilibrium time, h is the initial adsorption rate, $h = kq_e^2$, and k is the rate constant)

The Langmuir and Freundlich models were used to interpret the experimental data. The linear equation of the Langmuir isotherm model is expressed as followed:

$$\frac{C_e}{q_e}=\frac{1}{q_m k_L}+\frac{C_e}{q_m}$$

Where q_m is the maximum sorption capacity corresponding to complete monolayer coverage (mg/g) and k_L is a constant indirectly related to sorption capacity and energy of sorption (L/mg), which characterizes the affinity of the adsorbate with the adsorbent. The linearized plot was obtained when we plotted C_e/q_e against C_e and q_m and k_L could be calculated from the slope and intercept.

The linear equation of Freundlich isotherm model can be expressed by:

$$\ln q_e=\ln k_F+\frac{1}{n}\ln C_e$$

Where k_F and n are the Freundlich constants related to the sorption capacity and the sorption intensity, respectively. The linear plot was obtained by plotting $\ln q_e$ against $\ln C_e$, and the values of k_F and n were calculated from the slope and intercept of the straight line.
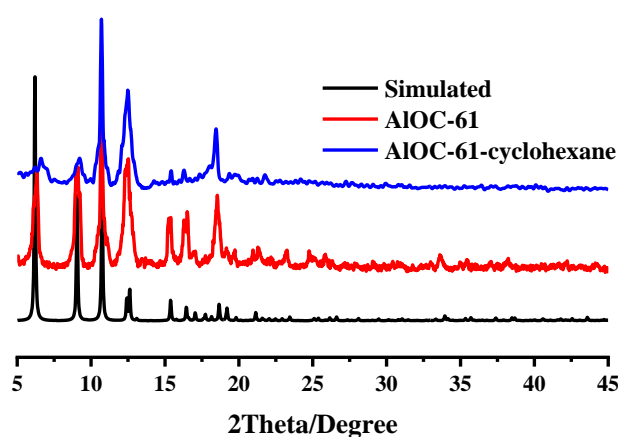

Fig. S27 PXRD patterns of **AlOC-61** in cyclohexane solution at room temperature for 24 h.
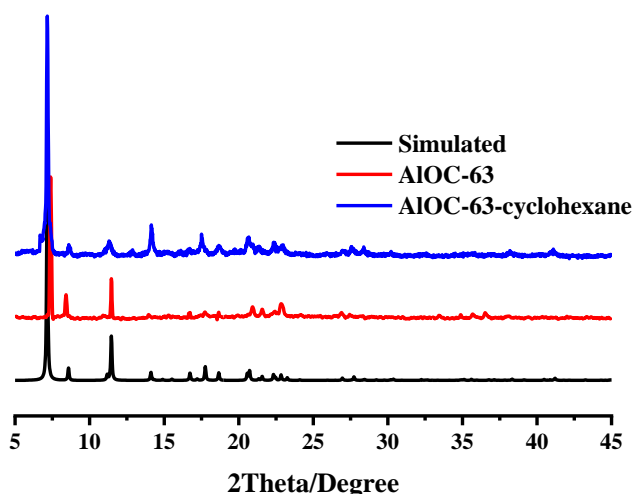

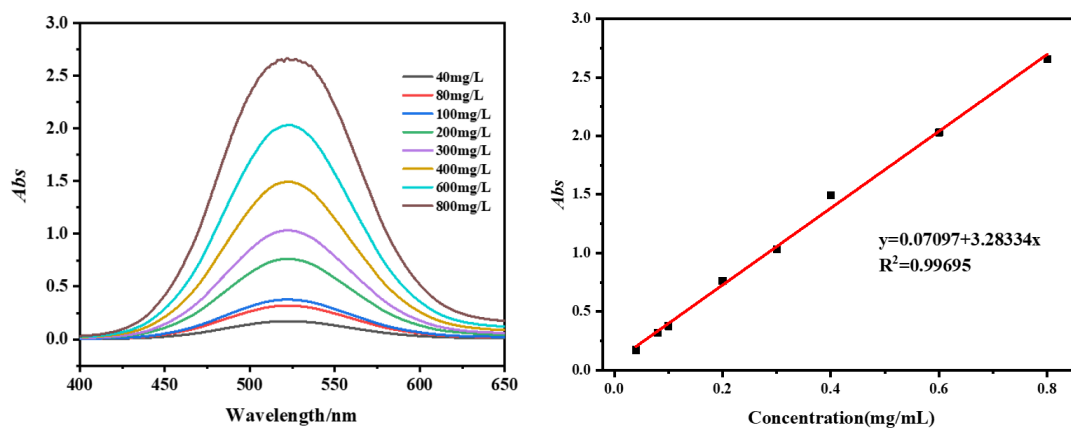**Fig. S28** PXRD patterns of **AlOC-63** in cyclohexane solution at room temperature for 24 h.

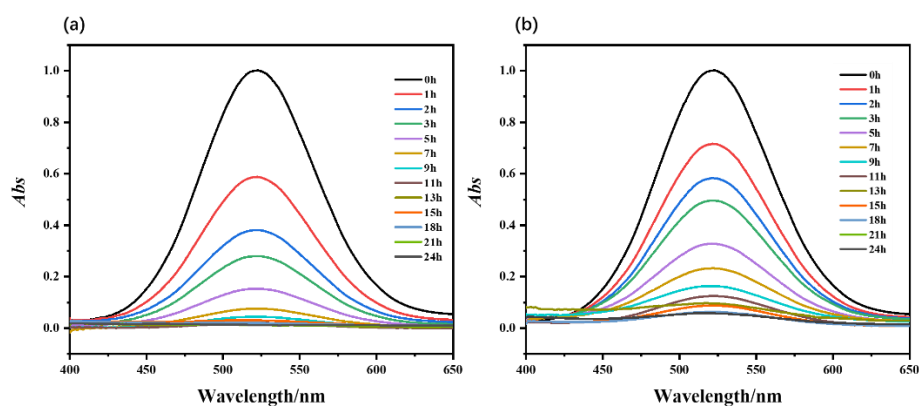**Fig. S29** Calibration plots of standard iodine by UV-vis spectra in cyclohexane solution.

Fig. S30 UV−vis spectra of **AlOCs** adsorbing iodine over time in a 1mmol·L^{-1} cyclohexane solution of iodine when 10 mg of **AlOCs** is added. (a) **AlOC-61**, (b) **AlOC-63**.

Table S2 Kinetic parameters of the pseudo-second-order model for iodine adsorption toward **AlOC-61**, **AlOC-63** (1mmol/L)

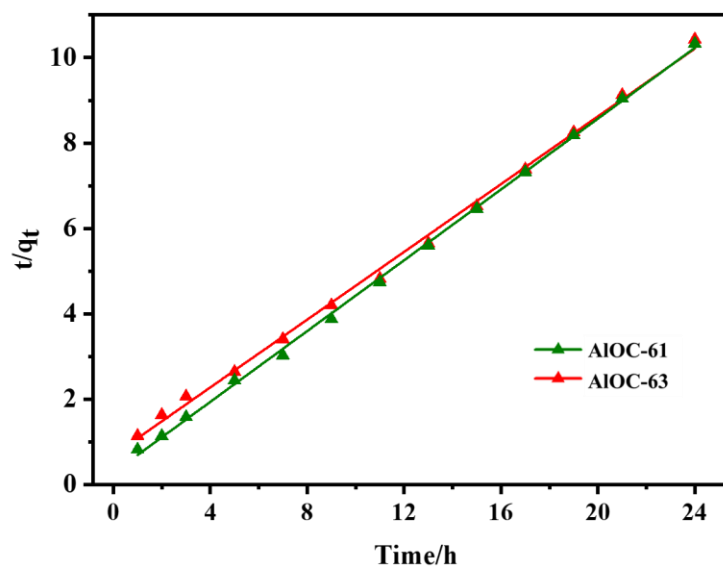| Sample	Second-order kinetic model			
	q_e (mg/g)	h (g mg^{-1}h^{-1})	k (g mg^{-1}h^{-1})	R^2
AlOC-61	241.117	359.145	6.173×10^{-3}	0.99909
AlOC-63	251.948	145.225	2.287×10^{-3}	0.99765

Fig. S31 The corresponding plots of pseudo-second-order kinetics of I_2 adsorption onto **AlOC-61** (olive green) and **AlOC-63** (red).

Table S3 Fitting results of the sorption isotherms according to the Langmuir equations and Freundlich equations

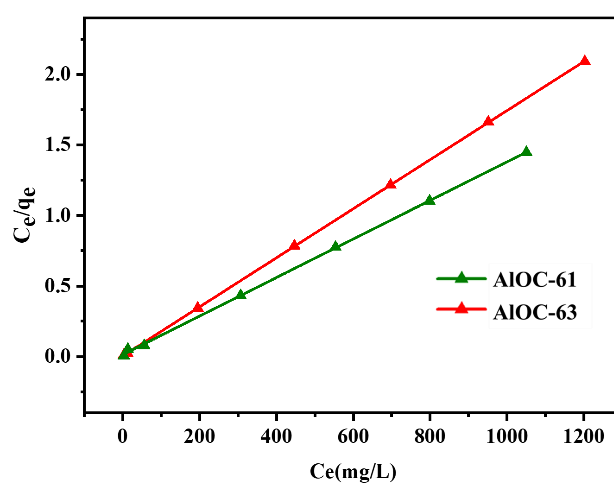| Sample	Langmuir			Freundlich		
	Q_m (mg/g)	K_L (L/mg)	R^2	k_F ($L^n/mol^{n-1}g$)	n	R^2
AlOC-61	732.44445	0.09675	0.98953	37.33766	2.41156	0.74737
AlOC-63	575.51794	0.33351	0.99861	56.66853	3.09831	0.82228

Fig. S32 The corresponding plots of the Langmuir model of **AlOC-61**(olive green) and **AlOC-63** (red).

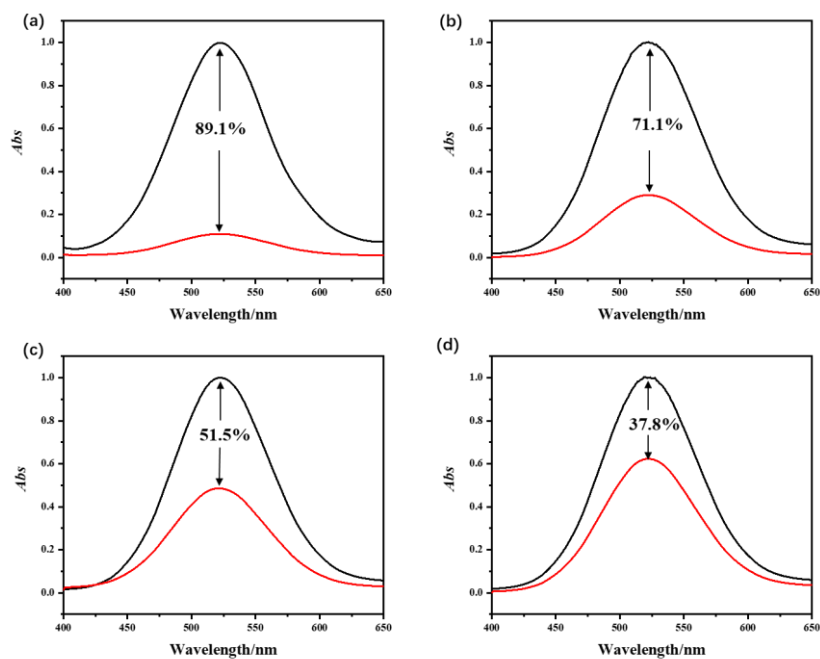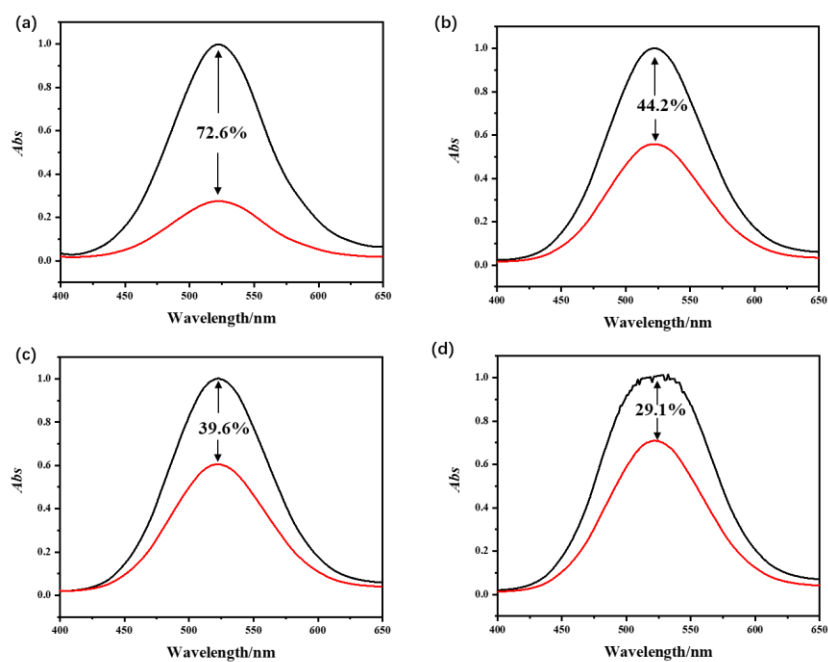**Fig. S33** UV-vis spectra of **AlOC-61** (10 mg) adsorbing iodine for 24 h in different concentration cyclohexane solution of iodine: (a) 3mmol·L⁻¹; (b) 4mmol·L⁻¹; (c) 5mmol·L⁻¹; (d) 6mmol·L⁻¹.

Fig. S34 UV-vis spectra of **AlOC-63** (10 mg) adsorbing iodine for 24 h in different concentration cyclohexane solution of iodine: (a) 3mmol·L⁻¹; (b) 4mmol·L⁻¹; (c) 5mmol·L⁻¹; (d) 6mmol·L⁻¹.
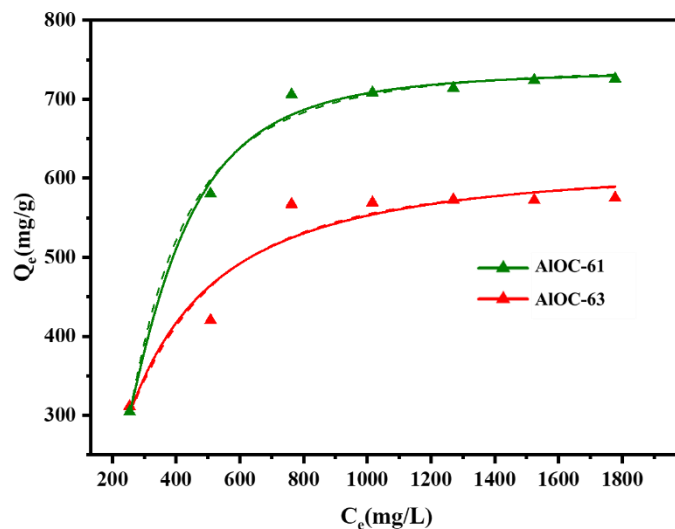
Fig. S35 Adsorption isotherms for the uptake of I$_2$ onto **AlOC-61** (olive green) and **AlOC-63** (red): Solid line, Langmuir fitting; dashed line, Freundlich fitting.
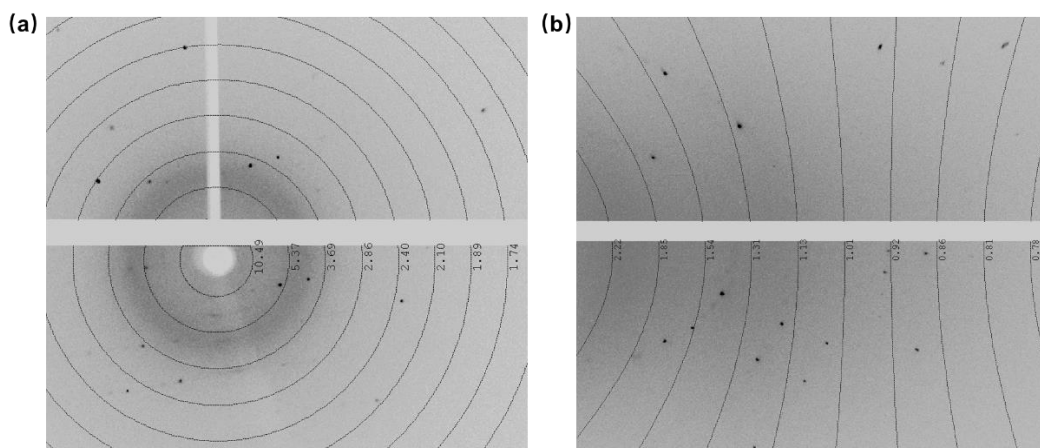

Fig. S36 SXRD patterns for **AlOC-61⊃I$_2$.**

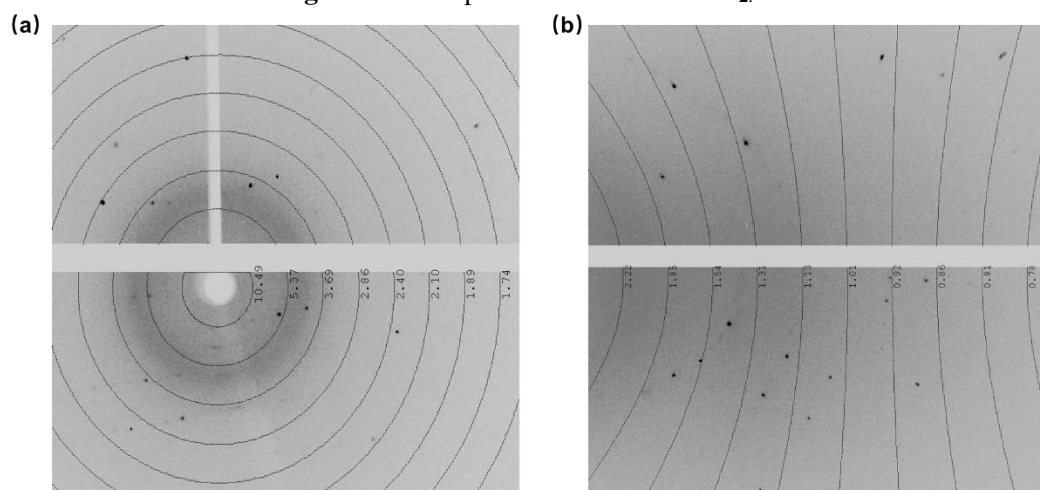
Fig. S37 SXRD patterns for **AlOC-63⊃I$_2$.**

The host-guest interaction between **AlOCs** and I$_2$ didn't make the crystal diffraction poorly. The existence of a good diffraction image point at a low angle and high angle confirms the good quality of **AlOCs** on a single crystalline state after the iodine adsorption.
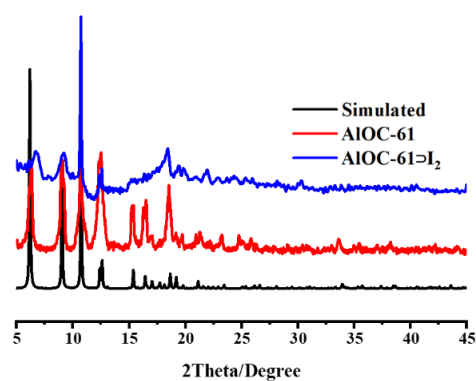
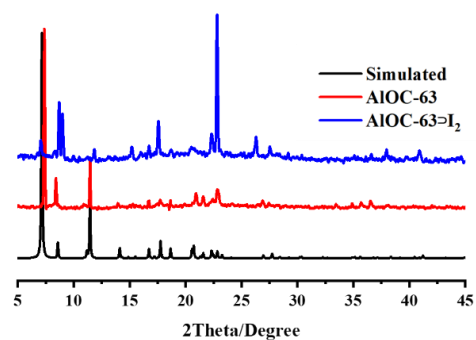**Fig. S38** PXRD patterns of **AlOC-61** before and after iodine adsorption.

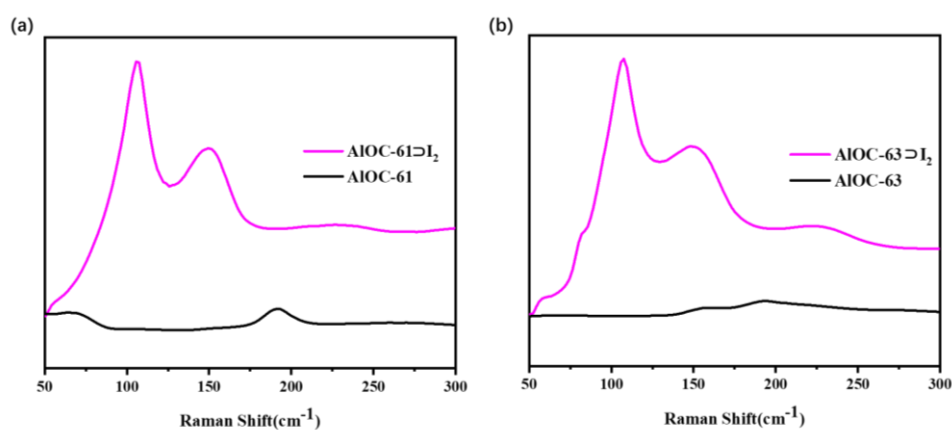**Fig. S39** PXRD patterns of **AlOC-63** before and after iodine adsorption.

Fig. S40 Comparison Raman spectra of bare samples and **AlOCs⊃I₂** in the low energy region. (**AlOCs⊃I₂** were obtained by soaking fresh samples in iodine/cyclohexane solutions (10 mL, 3mmol·L^{-1} for 24 hours).

Raman spectra confirmed the existence of iodine species in **AlOC-61⊃I₂** and **AlOC-63⊃I₂**. The new peak appeared at ~106, 148 cm^{-1} for **AlOC-61⊃I₂**. And the new peak appeared at ~107, 150 cm^{-1} for **AlOC-63⊃I₂**.
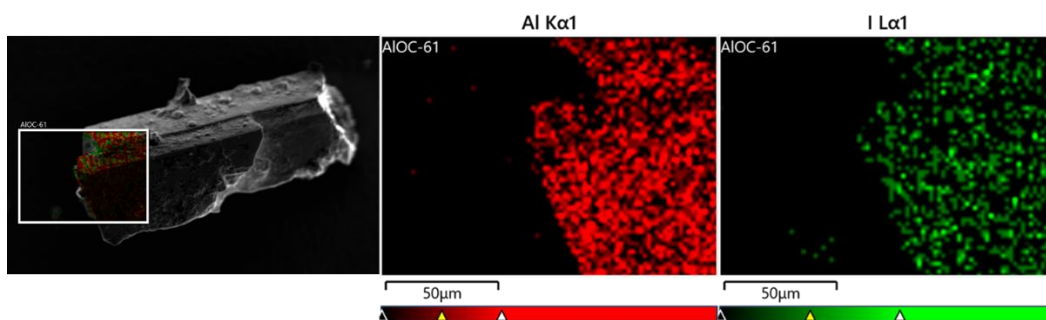
Fig. S41 EDS-mapping spectra of **AlOC-61⊃I₂**. From left to right are crystal appearance, aluminum, iodine elements.
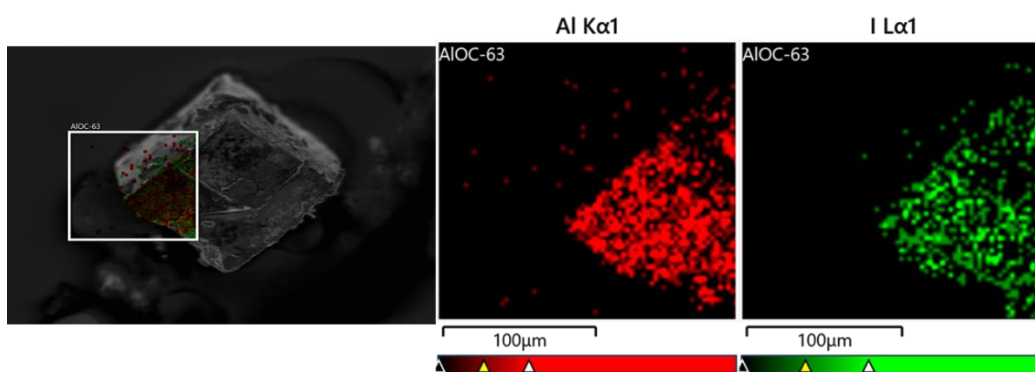

Fig. S42 EDS-mapping spectra of AlOC-63⊃I₂. From left to right are crystal appearance, aluminum, iodine elements.
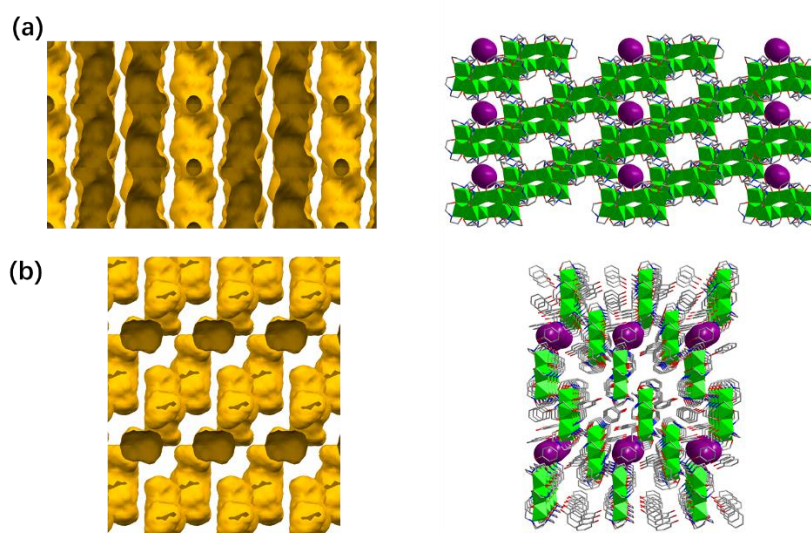

Fig. S43 According to the calculation results, simulate the position of one iodine molecule in the free void, and can observe the I_2 molecules get into the pores ((a) **AlOC-61** and (b) **AlOC-63**) by entering through the pocket.
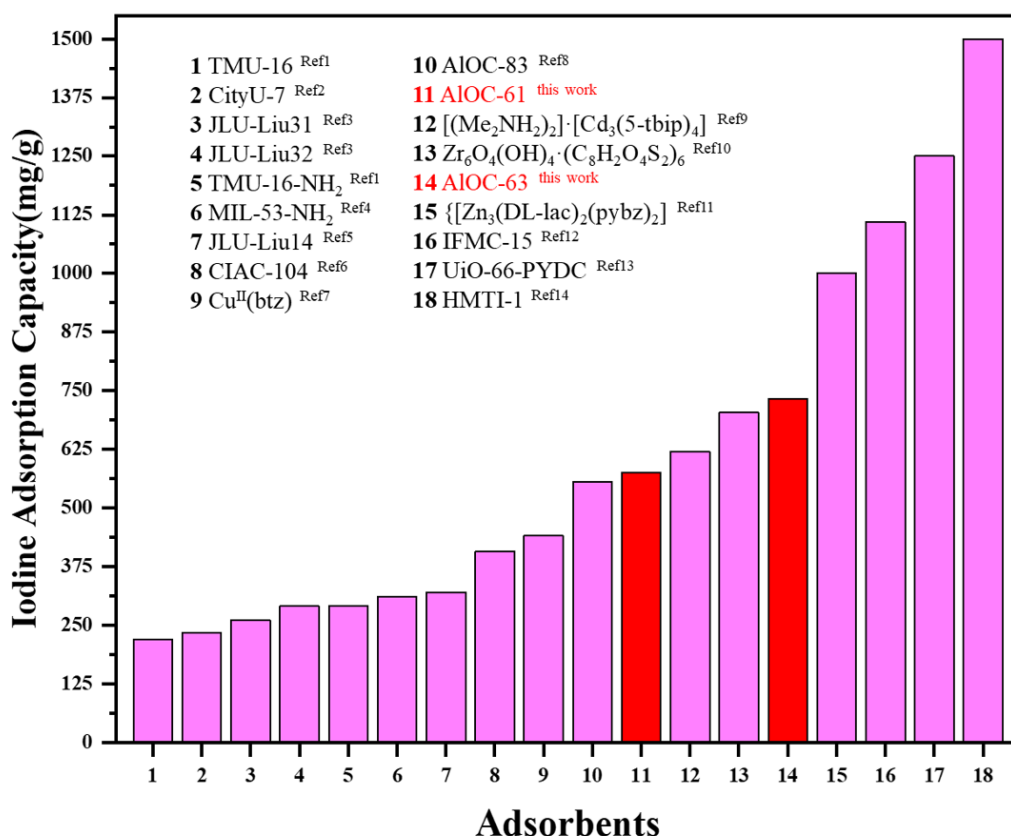
Fig. S44 Liquid phase iodine adsorption capacities of different adsorbents.[1-14]

DFT calculations.

All density functional theory calculations were implemented by the Dmol3 package.[15, 16] All calculations were performed with PBE exchange-correlation functional (the 1996 functional of Perdew, Burke and Ernzerhof) on periodically repeated slabs.[17] The double-numeric quality basis set with polarization functions (DNP) was adopted.[16, 18, 19] The numerical basis sets can minimise the basis-set superposition error.[20] A Fermi smearing of 0.005 hartree was utilized was used for structural relaxation. The tolerances of the energy, gradient and displacement convergence were 1×10^{-5} hartree, 2×10^{-3} hartree per Å, and 5×10^{-3} Å, respectively. In addition, the adsorption energy for iodine is estimated by the change of energy ΔE:

$$\Delta E = E_{\text{coordination}} - E_{I_2} - E_{AlOC}$$

Where $E_{\text{coordination}}$ is the optimized energy of the coordinated structures, E_{I2} and E_{AlOC} are the optimized energies of the I_2 and **AlOC** parts, respectively.

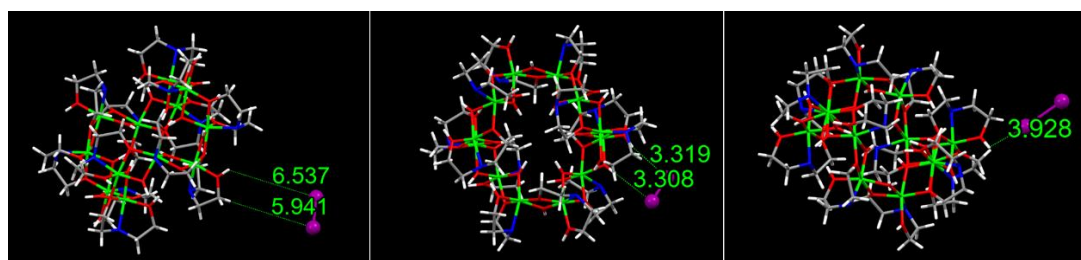**Optimized geometries of the AlOCs interacting with iodine molecules.**

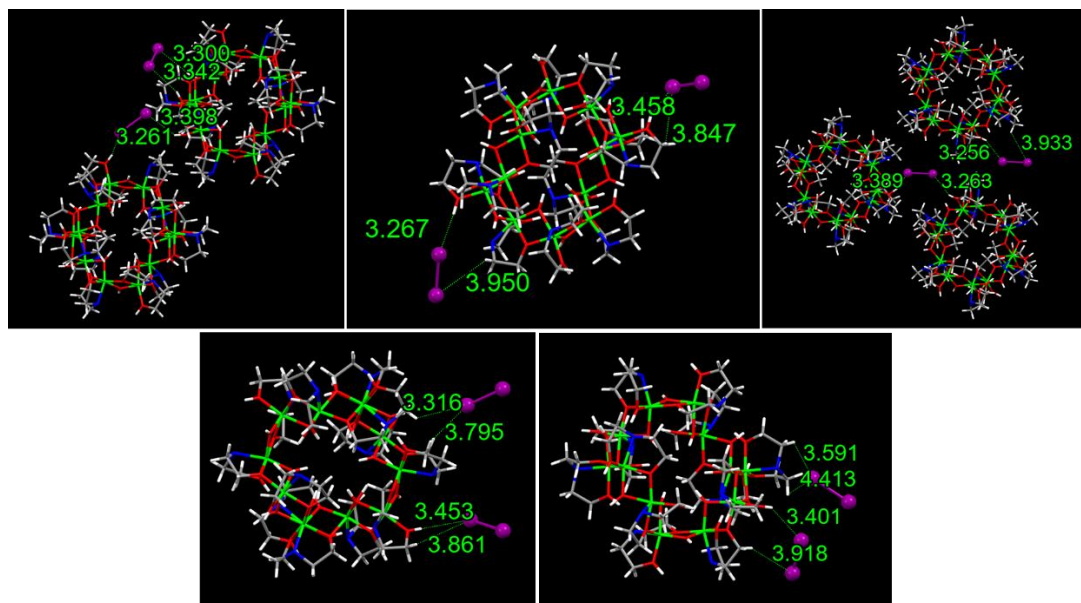**Fig. S45 AlOC-61** interacted with one iodine molecule.

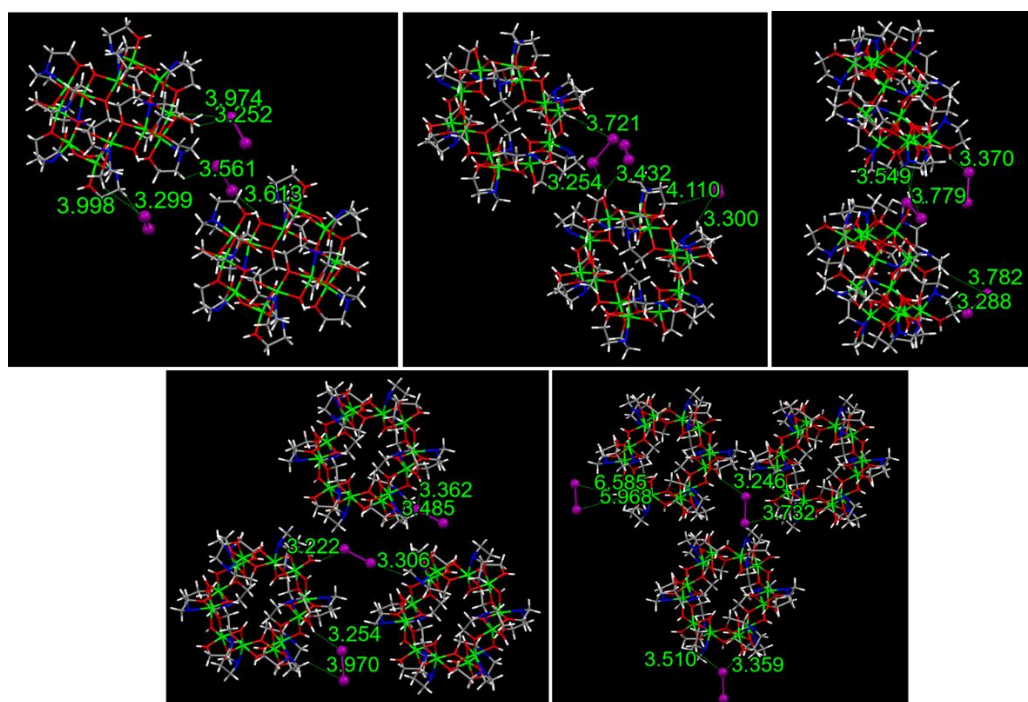
Fig. S46 AlOC-61 interacted with two iodine molecules.

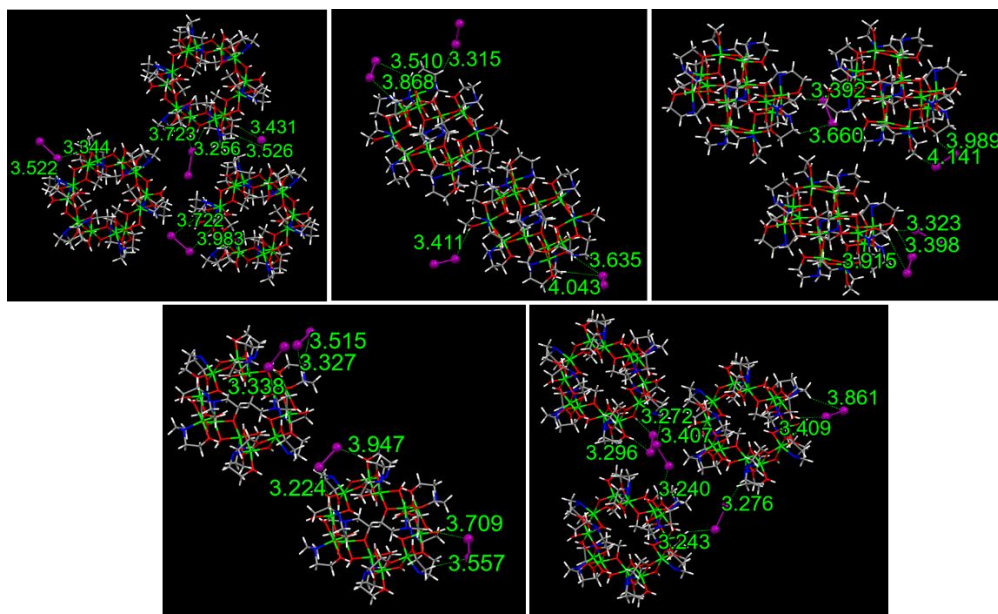**Fig. S47 AlOC-61** interacted with three iodine molecules.

Fig. S48 AlOC-61 interacted with four iodine molecules.
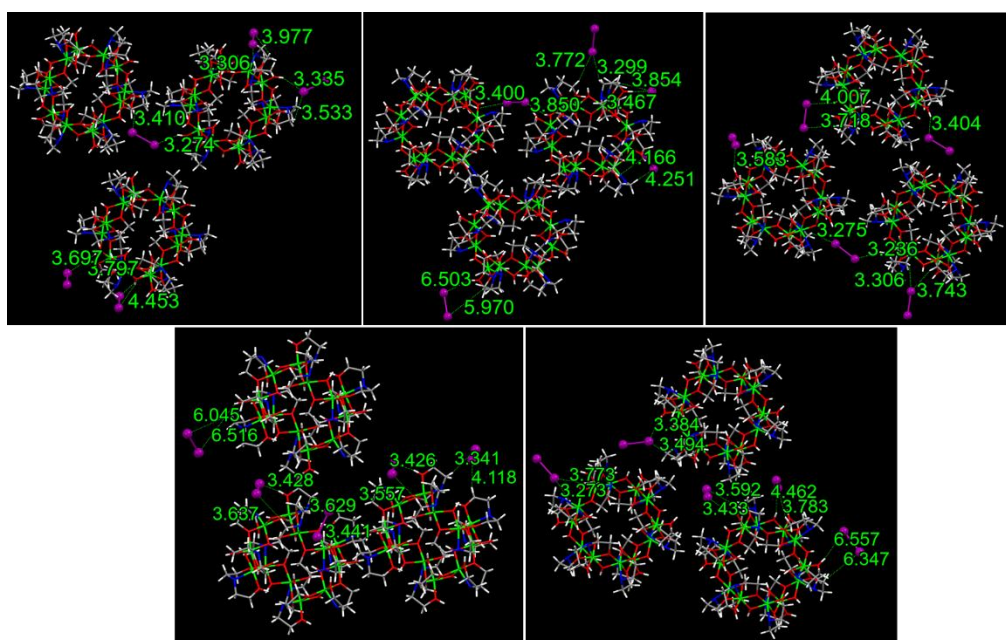

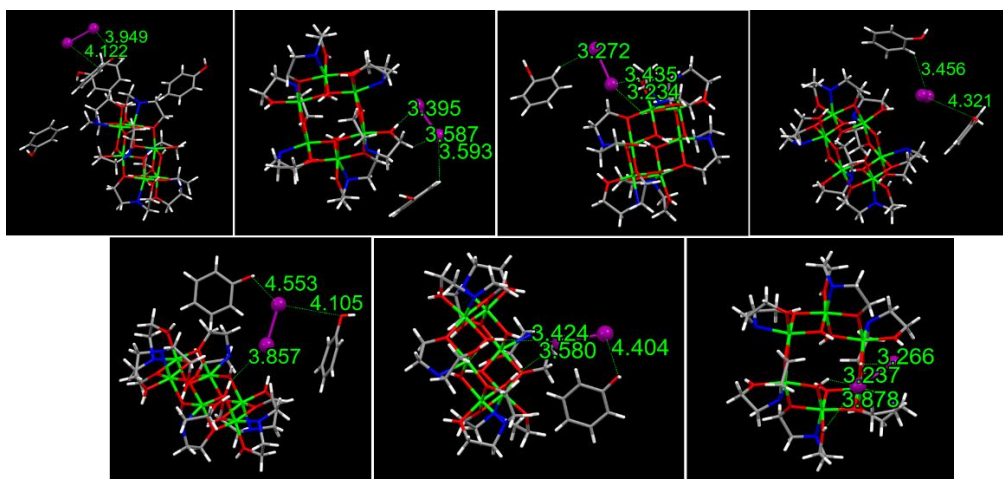**Fig. S49 AlOC-61** interacted with five iodine molecules.

Fig. S50 AlOC-63 interacted with one iodine molecule.

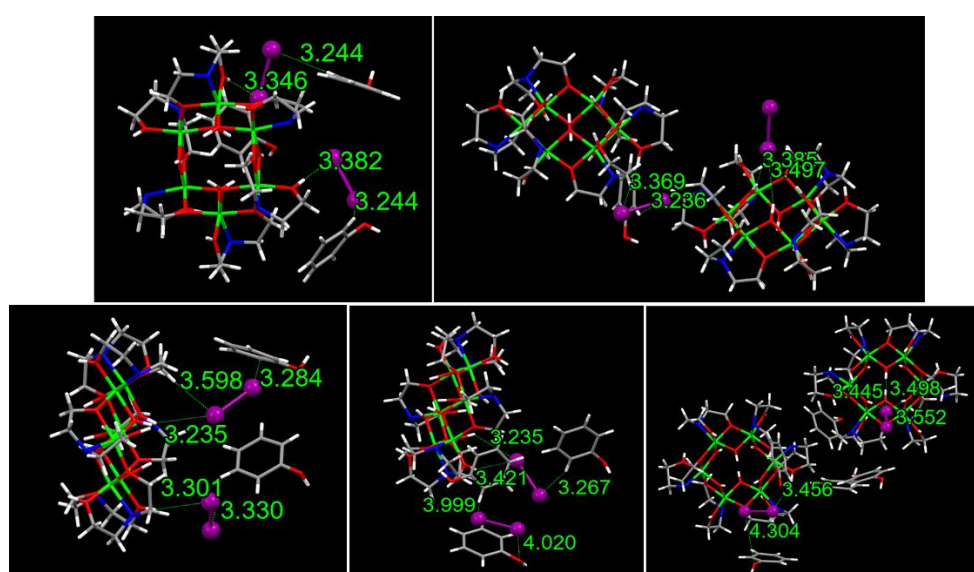
Fig. S51 AlOC-63 interacted with two iodine molecules.

Fig. S52 AlOC-63 interacted with three iodine molecules.

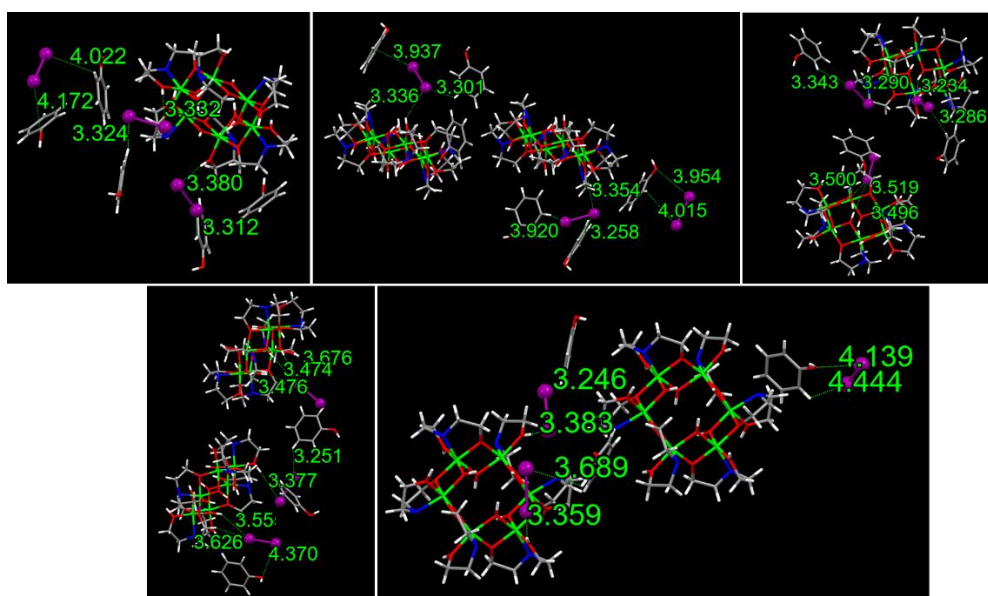**Fig. S53 AlOC-63** interacted with four iodine molecules.

Fig. S54 AlOC-63 interacted with five iodine molecules.

Reference

[1] V. Safarifard, A. Morsali, *CrystEngComm* **2014**, *16*, 8660-8663.

[2] J. Liu, R. Xiao, Y. L. Wong, X. P. Zhou, M. Zeller, A. D. Hunter, Q. Fang, L. Liao, Z. Xu, *Inorg. Chem.* **2018**, *57*, 4807-4811.

[3] S. Yao, X. Sun, B. Liu, R. Krishna, G. Li, Q. Huo, Y. Liu, *J. Mater. Chem. A* **2016**, *4*, 15081-15087.

[4] C. Falaise, C. Volkringer, J. Facqueur, T. Bousquet, L. Gasnot, T. Loiseau, *Chem. Commun.* **2013**, *49*, 10320-10322.

[5] J. Wang, J. Luo, X. Luo, J. Zhao, D.-S. Li, G. Li, Q. Huo, Y. Liu, *Cryst. Growth Des.* **2015**, *15*, 915-920.

[6] M. Liu, W. Liao, C. Hu, S. Du, H. Zhang, *Angew. Chem. Int. Ed.* **2012**, *51*, 1585-1588; *Angew. Chem.* **2012**, *124*, 1617-1620.

[7] P. Cui, L. Ren, Z. Chen, H. Hu, B. Zhao, W. Shi, P. Cheng, *Inorg. Chem.* **2012**, *51*, 2303-2310.

[8] C.-H. Liu, W.-H. Fang, Y. Sun, S. Yao, S.-T. Wang, D. Lu, J. Zhang, *Angew. Chem. Int. Ed.* **2021**, *60*, 21426-21433; *Angew. Chem.* **2021**, *133*, 21596-21603.

[9] A. K. Chaudhari, S. Mukherjee, S. S. Nagarkar, B. Joarder, S. K. Ghosh, *CrystEngComm* **2013**, *15*, 9465.

[10] K. K. Yee, Y. L. Wong, Z. Xu, *Dalton Trans.* **2016**, *45*, 5334-5338.

[11] M. H. Zeng, Q. X. Wang, Y. X. Tan, S. Hu, H. X. Zhao, L. S. Long, M. Kurmoo, *J. Am. Chem. Soc.* **2010**, *132*, 2561-2563.

[12] W. W. He, S. L. Li, G. S. Yang, Y. Q. Lan, Z. M. Su, Q. Fu, *Chem. Commun.* **2012**, *48*, 10001-10003.

[13] Z. Wang, Y. Huang, J. Yang, Y. Li, Q. Zhuang, J. Gu, *Dalton Trans.* **2017**, *46*, 7412-7420.

[14] L. Hashemi, A. Morsali, *CrystEngComm* **2012**, *14*, 779-781.

[15] B. Delley, *J. Chem. Phys.* **2000**, *113*, 7756-7764.

[16] B. Delley, *J. Chem. Phys.* **1990**, *92*, 508-517.

[17] J. P. Perdew, K. Burke, M. Ernzerhof, *Phys. Rev. Lett.* **1996**, *77*, 3865-3868.

[18] L. Versluis, T. Ziegler, *J. Chem. Phys.* **1988**, *88*, 322-328.

[19] U. von Barth, L. Hedin, *J. Phys. C: Sol. St. Phys.* **1972**, *5*, 1629-1642.

[20] N. Matsuzawa, J. e. Seto, D. A. Dixon, *J. Phys. Chem. A* **1997**, *101*, 9391-9398.